

# Lipid composition of microdomains is altered in a cell model of Gaucher disease

Leanne K. Hein,\* Stephen Duplock,\* John J. Hopwood,\*<sup>†</sup> and Maria Fuller<sup>1,\*</sup><sup>†</sup>

Lysosomal Diseases Research Unit,\* Department of Genetic Medicine, Children, Youth and Women's Health Service, North Adelaide, South Australia 5006; and Department of Pediatrics,<sup>†</sup> University of Adelaide, Adelaide, South Australia 5005

**Abstract** The formation of cholesterol and sphingolipids into specialized liquid-ordered membrane microdomains (rafts) has been proposed to function in the intracellular sorting and transport of proteins and lipids. Defined by biochemical criteria, rafts resist solubilization in nonionic detergents, enabling them to be isolated as detergent-resistant membranes (DRM). In this study, we characterized the lipid composition of DRM from a cell model of the sphingolipid storage disorder, Gaucher disease, in which the catabolism of the sphingolipid glucosylceramide (GC) is impaired. In this cell model, we showed that GC accumulated primarily in the DRM, with smaller secondary increases in ceramide, dihexosylceramide, trihexosylceramide, and phosphatidylglycerol. This suggested that not only was lipid metabolism altered as a consequence of the cells' inability to degrade GC, but this affected the DRM rather than other regions of the membrane. This increase in lipids in the DRM may be responsible for the altered lipid and protein sorting seen in Gaucher disease. Analysis of individual lipid species revealed preservation of the shorter and fully saturated fatty acid species in the DRM, suggesting that the highly ordered and tightly packed nature of the DRM is maintained.—Hein, L. K., S. Duplock, J. J. Hopwood, and M. Fuller. Lipid composition of microdomains is altered in a cell model of Gaucher disease. *J. Lipid Res.* 2008. 49: 1725–1734.

**Supplementary key words** membrane rafts • detergent-resistant membranes • mass spectrometry • glucosylceramide • lysosomal storage disorder • sphingolipids • phospholipids

The term “membrane rafts” [also referred to as lipid rafts and detergent-resistant membranes (DRM)] has been used to describe low-density membrane domains that are enriched in cholesterol, sphingolipids, and phospholipids containing predominately saturated fatty acids (1, 2). Membrane rafts exist in a liquid-ordered phase due to tight packing, which is achieved through the high proportion of saturated acyl chains present (3). These regions of

membrane are thought to play a role in many cellular functions, including cell proliferation and apoptosis (4, 5). Furthermore, these domains facilitate interactions among the lipid and protein components of signaling pathways, thereby regulating these processes (6). The lipid composition of the membrane rafts is highly specialized, and it is this unique composition that enables them to carry out their signaling role (7). Therefore, the cell must tightly regulate the composition of these membrane rafts by sphingolipid synthesis and degradation, and transport to and from the cell surface, to ensure their function.

The constitutive degradation of sphingolipids occurs in the acidic subcellular compartments, the endosomes and lysosomes. Inheritable disorders affecting proteins acting in the sphingolipid degradative pathways are known as the sphingolipidoses, which are characterized by the lysosomal accumulation of sphingolipids (8). A common defect in sorting and trafficking in the sphingolipidoses has been reported, based on the observation that a short acyl chain (BODIPY) derivative of lactosylceramide is mistargeted to late endosomes and lysosomes instead of to the Golgi apparatus in normal cells (9, 10). This altered trafficking can be reversed by depleting intracellular cholesterol, suggesting that the altered trafficking is related to the accumulation of cholesterol (11). This altered endocytic sorting is probably due to the accumulation of endocytic membrane rafts, which have been seen in fibroblasts from patients with these disorders (9, 12). The accumulation of membrane rafts in storage bodies may prevent their normal function by mislocalizing proteins involved in signaling and transport (12, 13).

Gaucher disease is an inborn error of sphingolipid metabolism caused by a deficiency of the lysosomal enzyme, acid

---

Abbreviations: Cer, ceramide; DHC, dihexosylceramide; DRM, detergent-resistant membranes; ESI-MS/MS, electrospray ionization tandem mass spectrometry; GC, glucosylceramide; HRP, horseradish peroxidase; PC, phosphatidylcholine; PG, phosphatidylglycerol; PI, phosphatidylinositol; PVDF, polyvinylidene fluoride; SM, sphingomyelin; THC, trihexosylceramide.

<sup>1</sup>To whom correspondence should be addressed.  
e-mail: maria.fuller@adelaide.edu.au

---

This work was supported by a National Health and Medical Research Council project grant in Australia.

Manuscript received 20 February 2008 and in revised form 9 April 2008.

Published, JLR Papers in Press, April 21, 2008.  
DOI 10.1194/jlr.M800092.JLR200

Copyright © 2008 by the American Society for Biochemistry and Molecular Biology, Inc.

This article is available online at <http://www.jlr.org>

$\beta$ -glucosidase, which is responsible for cleaving the sphingolipid, glucosylceramide (GC), into glucose and ceramide (Cer) (14). GC is composed of Cer, *D-erythro*-sphingosine, and a fatty acid commonly containing 16–26 carbon atoms in the acyl chain, with glucose attached through a glycosidic bond as the head group. GC is one of the sphingolipids found in membrane rafts, and has also been demonstrated to play a role in the endocytic sorting of sphingolipids and cholesterol, with amounts of these lipids altered in a macrophage model of Gaucher disease (15). This is most likely a consequence of the location and function of sphingolipids and cholesterol in membrane rafts.

In this report, we investigated what effect a block in GC degradation had on the lipid composition of membrane rafts in a cell model of Gaucher disease. Previously, we established a macrophage model of the disease and demonstrated that as well as increased GC concentrations, there was secondary accumulation of Cer, dihexosylceramide (DHC), trihexosylceramide (THC), and phosphatidylglycerol (PG) (16). Furthermore, we found that initially, GC and secondary lipid accumulation predominated in the lysosomes, but as more GC accumulated, the lipids distributed relatively evenly across the cell throughout other subcellular compartments. Here, we assessed whether lysosomal GC accumulation alters membrane microdomain composition by isolating detergent-soluble membranes and DRM from our Gaucher macrophage model. The sphingolipid and phospholipid composition of the membrane domains was analyzed by electrospray ionization tandem mass spectrometry (ESI-MS/MS) and shown to differ in the Gaucher disease cell model compared with control cells, thereby altering their lipid composition. Given the role of membrane rafts in signaling, their altered lipid composition is likely to disrupt their function.

## MATERIALS AND METHODS

### Materials

Ovalbumin, anti-flotillin 1 (polyclonal), cholesteryl heptadecanoate (cholesteryl ester), 17:0, and 1,2-dimyristoyl-*sn*-glycero-3-phosphocholine [phosphatidylcholine (PC), 14:0/14:0] were purchased from Sigma (St. Louis, MO). *N*-heptadecanoyl-*D-erythro*-sphingosine (Cer, 17:0) and 1,2-dimyristoyl-*sn*-glycero-3[phospho-*rac*-(1-glycerol) (PG), 14:0/14:0] were from Avanti Polar Lipids (Alabaster, AL). *N*-palmitoyl-*d*<sub>3</sub>-glucosylsphingosine, 16:0(*d*<sub>3</sub>), *N*-palmitoyl-*d*<sub>3</sub>-lactosylceramide 16:0(*d*<sub>3</sub>), and phosphatidylinositol (PI), 16:0/16:0 were purchased from Matreya LLC (Pleasant Gap, PA). HRP-conjugated sheep anti-rabbit immunoglobulin was purchased from Chemicon (Victoria, Australia). The ECL Western blotting analysis system was purchased from GE Healthcare (Buckinghamshire, UK). Polyvinylidene fluoride (PVDF) transfer membrane was purchased from Perkin Elmer (Waltham, MA). All solvents were of HPLC grade, except chloroform, which contained 1% ethanol and was reagent grade, and were used without further purification.

### Gaucher disease macrophage model

THP-1 cells (human monocytic cell line) were differentiated into macrophages with phorbol 12-myristate 13-acetate, and the Gaucher disease phenotype was induced with conduritol B epox-

ide as described previously (16). Following 10 days in culture, THP-1 macrophages were harvested into PBS using a cell scraper and washed twice with PBS, and membrane microdomains were isolated from the cell pellets.

### Preparation of membrane microdomains

Membrane microdomains were prepared from four T<sub>75</sub> flasks of THP-1 macrophages using the method of Lisanti et al. (17). Briefly, cell pellets were resuspended in 2 ml MBS buffer (25 mM MES, pH 6.5, 0.15 M NaCl), containing 1% (v/v) Triton X-100 and 1 mM PMSF, and then homogenized with 12 strokes of a Dounce homogenizer and incubated on ice for 30 min. A 50  $\mu$ l aliquot of the homogenized sample was taken for total cell protein determination by the method of Lowry et al. (18). The sucrose concentration in the cell extracts was adjusted to 40% (w/v) by adding 2 ml of 80% (w/v) sucrose in MBS containing 1% (v/v) Triton X-100 and 1 mM PMSF before being placed in the bottom of a Beckman (Palo Alto, CA) centrifuge tube (14 mm  $\times$  95 mm). The sample was overlaid with 5 ml of 30% (w/v) sucrose in MBS (without Triton X-100), followed by 3 ml of 5% (w/v) sucrose in MBS (without Triton X-100). Samples were centrifuged at 270,500 *g* for 16–20 h using a swing-out rotor. One milliliter fractions (12 in total) were collected from the top of the gradient.

### Isolation of DRM from lysosomes

Subcellular fractionation was performed on eight T<sub>75</sub> flasks of THP-1 macrophages, and lysosomes were identified by  $\beta$ -hexosaminidase activity as previously described (16). The lysosomal fractions were pooled, and DRM were isolated as above, with the following modifications. Triton X-100 was added to each 3 ml lysosomal fraction to give a final concentration of 1% (v/v), followed by the addition of 320  $\mu$ l of MBS buffer containing 1% (v/v) Triton X-100 and 1 mM PMSF. The samples were homogenized with 12 strokes of a Dounce homogenizer and incubated on ice for 30 min. The sucrose concentration of the samples was adjusted to 40% (w/v) by the addition of 2.65 ml of 80% (w/v) sucrose [assuming that the pooled lysosomal fractions had a sucrose concentration of approximately 8.5% (w/v)] in MBS containing 1% (v/v) Triton X-100 and 1 mM PMSF and then placed in the bottom of a Beckman centrifuge tube (14 mm  $\times$  95 mm). Each sample was overlaid with 4.5 ml of 30% (w/v) sucrose in MBS (without Triton X-100), followed by 1.5 ml of 5% (w/v) sucrose in MBS (without Triton X-100), centrifuged, and 12 fractions collected as described above.

### Western blot analysis on membrane microdomains

Aliquots (350  $\mu$ l) of each membrane microdomain fraction were precipitated with the addition of 4  $\mu$ l of 2% sodium deoxycholate and incubated on ice for 15 min. Cold TCA (24%) was added to each sample to give a final concentration of 6%, and samples were incubated on ice for a further 30 min. Samples were then centrifuged at 16,060 *g* for 30 min at 4°C. The supernatant was removed, and the pellet was resuspended in 1 ml of 1% triethylamine (v/v) in acetone and centrifuged for an additional 5 min. The triethylamine wash was repeated before the pellet was resuspended in 1 ml of diethyl ether and centrifuged again for 5 min. Precipitated samples were resuspended in sample buffer and electrophoresed on 10% SDS-PAGE by the method of Laemmli (19). The gel was transferred to PVDF membrane at 0.5 A for 1 h in transfer buffer (10 mM 3-[cyclohexylamino]-1-propanesulfonic acid, pH 11, containing 10% methanol). The membrane was washed three times for 5 min in wash solution [0.1% (w/v) skim milk, 0.1% (w/v) ovalbumin, and 0.4% (v/v)

Tween-20 in PBS] and then blocked in 1 M glycine, 5% (w/v) skim milk, and 1% (w/v) ovalbumin for 1 h at room temperature. After the membrane was washed again, rabbit polyclonal antibody against flotillin 1 (2 µg/ml in wash solution) was added and incubated overnight at 4°C. The membrane was then washed three times for 5 min in wash solution before the addition of HRP-conjugated sheep anti-rabbit immunoglobulin and incubated for 1 h at room temperature. The membrane was washed again three times for 5 min before a final wash for 5 min in 0.02 M Tris, pH 7, and 0.25 M NaCl, and developed using the ECL Western blotting analysis system.

### Lipid extractions of membrane microdomain fractions

Lipids were extracted from membrane microdomain fractions (500 µl) according to the method of Bligh and Dyer (20), and made up to 750 µl with H<sub>2</sub>O. Each sample was extracted with 2.8 ml of CHCl<sub>3</sub>-MeOH (1:2) containing 400 pmol of each of the following internal standards: Cer 17:0, GC 16:0(*d*<sub>3</sub>), DHC 16:0(*d*<sub>3</sub>), PC 14:0/14:0, PG 14:0/14:0, PI 16:0/16:0, and cholesterol ester 17:0. The mixture was shaken for 10 min and allowed to stand at room temperature for 50 min. The samples were partitioned by the addition of 950 µl CHCl<sub>3</sub> and 950 µl H<sub>2</sub>O and shaken for 10 min prior to centrifugation at 2,300 *g* for 5 min. The upper phase was discarded, and the lower phase was transferred to a new glass tube and washed with 0.5 ml Bligh-Dyer synthetic upper phase [prepared by mixing 15 ml H<sub>2</sub>O with 56 ml CHCl<sub>3</sub>-MeOH (1:2), shaking vigorously for 1 min before adding 19 ml CHCl<sub>3</sub> followed by 19 ml H<sub>2</sub>O, and shaking again; the mixture was then allowed to stand at room temperature overnight, and the top aqueous layer was retained for use as the synthetic upper phase], mixed for 10 min, and centrifuged at 2,300 *g* for 5 min. The upper phase was discarded, and the lower, hydrophobic phase was dried under a gentle stream of N<sub>2</sub> at 40°C. To remove detergent, the dried extracts were resuspended in 20 µl MeOH and 180 µl CHCl<sub>3</sub> and mixed, prior to placing them onto a silica reverse-phase column (United Chemical Technologies; Bristol, PA) that had been preconditioned with 3 ml MeOH, followed by 3 ml CHCl<sub>3</sub>. Once the sample had completely entered the solid phase, the columns were washed with 3 ml CHCl<sub>3</sub>, and the sphingolipids and phospholipids were eluted from the columns with 3 ml MeOH and collected into clean glass tubes. The samples were then dried under a gentle stream of N<sub>2</sub> at 40°C.

### Quantification of lipids

Sphingolipid and phospholipid analysis was performed by ESI-MS/MS using a PE Sciex API 3000 triple quadrupole mass spectrometer with a turbo-ion spray source (200°C) and Analyst 1.1 data system. Prior to analysis, the dried extracts were resuspended in 100 µl MeOH, and two 50 µl aliquots were plated into microtitre wells. For phospholipid analysis, 50 µl MeOH was added to one aliquot, and 50 µl MeOH containing 20 mM HCOONH<sub>4</sub> was added to the other aliquot for sphingolipid analysis. Samples (20 µl) were injected into the electrospray source with a Gilson (Middleton, WI) 233 autosampler using MeOH as the carrying solvent at a flow rate of 80 µl/min. N<sub>2</sub> was used as the collision gas at a pressure of  $2 \times 10^{-5}$  Torr. Quantification of GC 18:1/16:0, 18:1/18:0, 18:1/20:0, 18:1/22:0, 18:1/24:0, 18:1/24:1, Cer 18:1/16:0, 18:1/20:0, 18:1/20:1, 18:1/23:0, 18:1/23:1, 18:1/24:0, 18:1/24:1, DHC 18:1/16:0, 18:1/20:0, 18:1/22:0, 18:1/22:0-OH, 18:1/24:0, 18:1/24:1, THC 18:1/16:0, 18:1/18:0, 18:1/20:0, 18:1/22:0, 18:1/24:0, 18:1/24:1, sphingomyelin (SM) 18:1/16:0, 18:1/16:1, 18:1/18:0, 18:1/18:1, 18:1/22:0, 18:1/24:0, 18:1/24:1, PC 32:0, 32:1, 34:1, 34:2, 36:2, 36:4, 38:4 (only the total number of carbons and double bonds of the two fatty acids are re-

ported), PI 16:0/18:0, 16:0/20:4, 18:0/18:0, 18:0/18:1, 18:0/20:3, 18:0/20:4, 18:0/22:5, 18:1/18:1, 18:1/20:4, and PG 16:0/18:1, 16:0/22:6, 16:1/20:4, 18:1/18:0, 18:1/18:1, 18:1/18:2, 18:1/20:4, 18:1/22:5, 18:1/22:6, 18:2/22:6, 20:4/22:6, 22:5/22:5, 22:6/22:5, 22:6/22:6 was performed using multiple-reaction monitoring. Each ion pair was monitored for 100 ms with a resolution of 0.7 amu at half-peak height and averaged from continuous scans over the injection period. GC, Cer, DHC, and THC were quantified in positive-ion mode using the *m/z* product ion of 264 corresponding to the sphingosine base, and PC and SM used the *m/z* product ion of 184 corresponding to the phosphocholine head group. PG and PI were quantified in the negative-ion mode with PG using the *m/z* product ion of 281 for 18:1/18:0, 18:1/18:1, 18:1/18:2, 18:1/22:5, and 18:1/22:6; 255 for 16:0/18:1 and 16:0/22:6; 303 for 18:1/20:4 and 20:4/22:6; 253 for 16:1/20:4; 279 for 18:2/22:6; 327 for 22:6/22:6; and 329 for 22:5/22:5 and 22:6/22:5, corresponding to the 18:1, 16:0, 20:4, 16:1, 18:2, 22:6, and 22:5 fatty acids, respectively. PI used the *m/z* product ion of 283 for 16:0/18:0, 18:0/18:0, 18:0/18:1, 18:0/20:3, 18:0/20:4, and 18:0/22:5; 281 for 18:1/18:1 and 18:1/20:4; and 255 for 16:0/20:4, corresponding to the 18:0, 18:1, and 16:0 fatty acids, respectively. Concentrations of each molecular species were calculated by relating the peak heights of each species to the peak height of the corresponding internal standard, with the THC and SM species being related to the DHC 16:0(*d*<sub>3</sub>) and PC 14:0/14:0, respectively. The total amount of each lipid type was calculated by summing the individual species in each class.

Cholesterol was determined in each of the membrane microdomain fractions following lipid extraction by the method of Bligh and Dyer (20) (without silica columns). The cholesterol ester 17:0 internal standard (400 pmol) was added to each sample. Cholesterol in each sample was converted to cholesterol ester by addition of 200 µl acetyl chloride-CHCl<sub>3</sub> (1:5; v/v) and analyzed by ESI-MS/MS as described by Liebisch et al. (21). Relative cholesterol levels were determined by relating the peak height of cholesterol to the peak height of the internal standard.

### Immune quantification of lysosomal proteins in the membrane microdomain fractions

The distribution of 11 lysosomal proteins, including β-glucosidase, LAMP-1, saposin C, α-iduronidase, sulphamidase, iduronate-2-sulphatase, acid sphingomyelinase, α-galactosidase, arylsulphatase A, *N*-acetylgalactosamine-4-sulphatase, and α-glucosidase were measured in 5 µl of each membrane microdomain fraction using a multiplex immune quantification assay as previously described (22).

## RESULTS

### Characterization of DRM

First, the membrane microdomain fractions containing DRM were identified based on Western blot analysis for the DRM marker, flotillin 1. **Figure 1A** shows that although flotillin 1 was present in fractions 3 through to 12 of the Gaucher cell model, the majority of flotillin 1 clearly resided in fractions 3 and 4. Untreated THP-1 macrophages showed the same distribution of flotillin 1 as the Gaucher cell model (data not shown). The DRM were further characterized by the distribution of cholesterol across the membrane microdomain fractions. Cholesterol predominated in the DRM (fractions 3 and 4) as well as the soluble

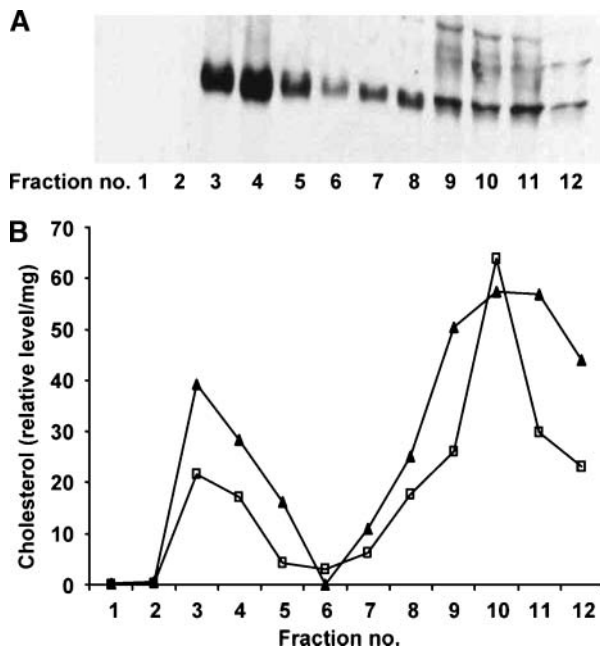


**Fig. 1.** Flotillin 1 and cholesterol in membrane microdomains from THP-1 macrophages. Membrane microdomains were isolated into 12 fractions from the Gaucher cell model, and 350  $\mu$ l of each fraction was TCA precipitated and analyzed by Western blot for flotillin 1 (A). Cholesterol in the membrane microdomain fractions was converted to cholesteryl ester using acetyl chloride and measured by electrospray ionization tandem mass spectrometry (ESI-MS/MS). B: The relative level and distribution of cholesterol in untreated THP-1 macrophages (closed triangles) and the Gaucher cell model (open squares). Relative cholesterol levels are expressed as a ratio of the 2:0 cholesteryl ester to the 17:0 cholesteryl ester internal standard per mg of total protein. Detergent-resistant membranes (DRM) are localized to fractions 3 and 4 and detergent-soluble membranes are found in fractions 7 to 12.

membrane domains (fractions 7 to 12) in both THP-1 macrophages and the Gaucher cell model (Fig. 1B).

#### Lipid composition of the membrane microdomains

Concentrations of Cer, GC, DHC, THC, SM, PC, PG, and PI were determined in each of the membrane microdomain fractions using ESI-MS/MS. The total amount of each of these lipid types was determined by summing each of the fatty acid species measured in each class. **Figure 2** shows that the DRM (fractions 3 and 4) were made up predominantly of PC, SM, Cer, and GC (approximately 49%, 27%, 8%, and 8%, respectively), whereas DHC, THC, PG, and PI each made up less than 3%. Assessment of the distribution of these lipids across the gradient revealed that GC, DHC, and THC resided predominantly in the DRM, whereas Cer, SM, and PC predominated in the soluble domains (fractions 7 to 12) and PI and PG were virtually absent from the DRM (Fig. 2A, B). The soluble domains (fractions 7 to 12) were composed primarily of PC, SM, PI, and Cer (approximately 75%, 11%, 8%, and 4%, respectively), whereas GC, DHC, THC, and PG each made up less than 1% (Fig. 2A, B).

The individual species of GC, DHC, THC, and Cer ranging from a 16 to a 24 carbon length fatty acid, displayed

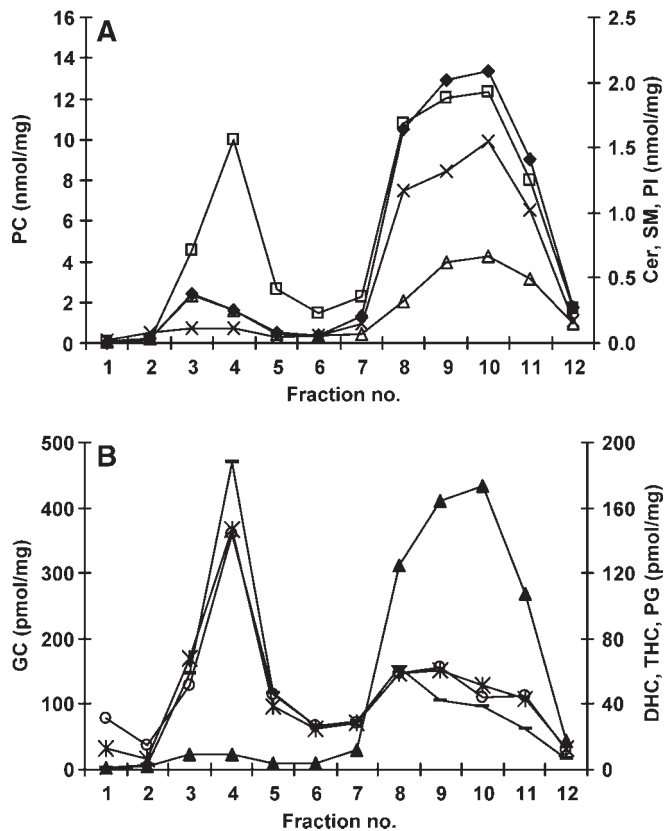


**Fig. 2.** Total lipid composition across the membrane microdomains in THP-1 macrophages. Lipids in each membrane microdomain fraction were extracted and measured by ESI-MS/MS. Individual species of phosphatidylcholine (PC) (closed diamonds), ceramide (Cer) (open triangles), sphingomyelin (SM) (open squares), and phosphatidylinositol (PI) (x) were summed to give total amounts, and these are shown in A. Individual species of glucosylceramide (GC) (-), dihexosylceramide (DHC) (\*), trihexosylceramide (THC) (open circles), and phosphatidylglycerol (PG) (closed triangles) were summed and are shown in B. Results are expressed as nanomoles or picomoles per milligram of total protein loaded onto the sucrose gradient prior to fractionation.

the same distribution in both the DRM and soluble domains; the most-abundant lipid species are depicted in **Fig. 3A–D** for illustration. The one species with a double bond (18:1/24:1), although being the minor species in the DRM, also distributed similarly to the 18:1/16:0, 18:1/22:0, and 18:1/24:0. However, for Cer, the ratio of the 18:1/16:0 to the 18:1/24:0 differed in the DRM and soluble domains, with 18:1/24:0 and 18:1/16:0 the most intense in the DRM and soluble domains, respectively (Fig. 3D). This was also true for the DHC species, albeit to a lesser extent (Fig. 3B). The distribution of the individual fatty acid species of SM differed across the membrane microdomains. Figure 3E shows that the 18:1/16:0 and 18:1/24:0 were the two most-intense species in the DRM and the two least-abundant in the soluble domains. Conversely, the 18:1/22:0 and 18:1/24:1 predominated in the soluble domains and were the less-intense species in the DRM. The other SM species (18:1/16:1, 18:1/18:0, and 18:1/18:1) were present in much smaller amounts. All PC species were found predominately in the soluble

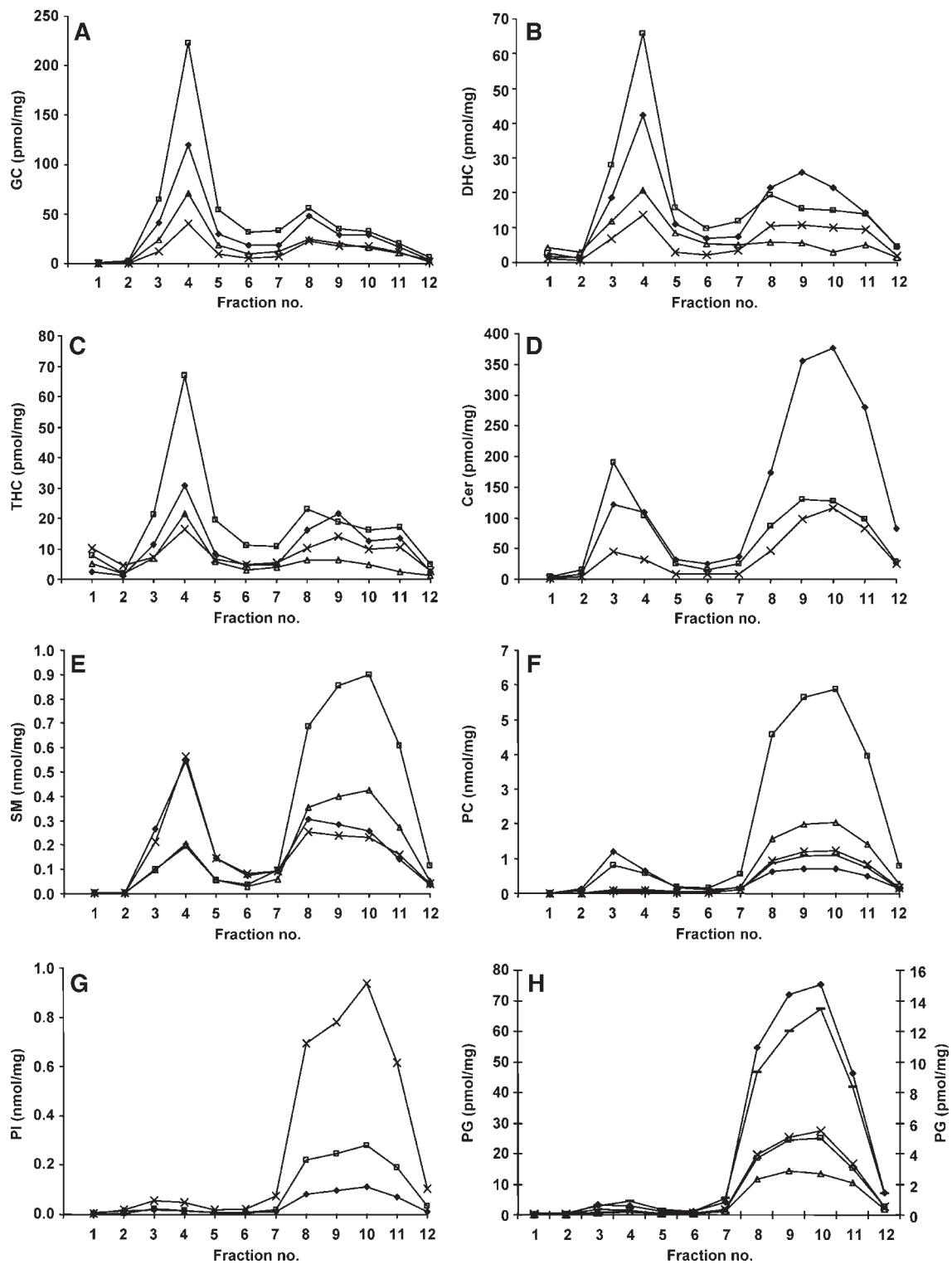


**Fig. 3.** Individual fatty acid species in the membrane microdomains of THP-1 macrophages. Membrane microdomains were isolated from THP-1 macrophages and 18:1/16:0 (closed diamonds), 18:1/22:0 (open triangles), 18:1/24:0 (open squares), and 18:1/24:1 (x) species of GC (A), DHC (B), and THC (C) are depicted across the 12 fractions. The individual Cer species 18:1/16:0 (closed diamonds), 18:1/24:0 (open squares) and 18:1/24:1 (x) are shown in D. Individual species of SM 18:1/16:0 (closed diamonds), 18:1/22:0 (open squares), 18:1/24:0 (x) and 18:1/24:1 (open triangles) are displayed in E, and individual species of PC 32:0 (closed diamonds), 34:1 (open squares), 34:2 (x), 36:2 (open triangles) and 38:4 (-) are displayed in F. PI 18:0/18:1 (closed diamonds), 18:0/20:3 (open squares) and 18:0/20:4 (x) are shown in G, and PG 16:0/18:1 (closed diamonds), 18:1/18:0 (open squares), 18:1/18:1 (x), 18:1/20:4 (open triangles, right-hand axis), and 18:1/22:6 (-, right-hand axis) in H. Results are expressed as nanomoles or picomoles per milligram of total protein loaded onto the sucrose gradient prior to fractionation.

membrane fractions, except for the saturated PC 32:0 (Fig. 3F). PC 32:0 was the major PC species in the DRM and the minor species in the soluble domains, and the only other species at appreciable levels in the DRM was the 34:1. The PC species with more than one double bond (PC 34:2, 36:2, and 38:4) were virtually excluded from the DRM (Fig. 3F). PC 32:1 and 36:4 were found in amounts similar to the PC 34:2 and 38:4 species and showed the same distribution (data not shown). The individual fatty acid species of PI and PG showed no difference in distribution in the DRM and soluble domains, and all species were virtually absent from the DRM (Fig. 3G, H, data not shown).

#### GC accumulation and lysosomal protein distribution in the membrane microdomains of the Gaucher disease macrophage model

DRM were isolated from untreated THP-1 macrophages and from the Gaucher macrophage model. All of the individual GC species were dramatically increased in the DRM and, to a smaller extent, in the soluble membrane domains in the Gaucher disease macrophage model (Fig. 4A–C and data not shown). GC 18:1/16:0, 18:1/24:0, 18:1/24:1, 18:1/18:0, 18:1/20:0, and 18:1/22:0 increased 23-, 16-, 28-, 23-, 19-, and 18-fold, respectively in the DRM of the cell model compared with untreated cells (Fig. 4A–C and data not shown). In the soluble membrane domains, the increase in GC species was on the order of 4- to 7-fold.

The distribution of 11 lysosomal proteins across the membrane microdomains was examined in the Gaucher macrophage model. All 11 lysosomal proteins measured ( $\beta$ -glucosidase, LAMP-1, saposin C,  $\alpha$ -iduronidase, sulphamidase, iduronate-2-sulphatase, acid sphingomyelinase,  $\alpha$ -galactosidase, arylsulphatase A, *N*-acetylgalactosamine-4-sulphatase, and  $\alpha$ -glucosidase) were shown to reside in the soluble membrane fractions of the Gaucher cell model (Fig. 4D). The same distribution was seen in untreated THP-1 macrophages (data not shown).

#### Lipid composition of DRM and soluble membrane domains in the Gaucher disease cell model

Along with a 20-fold increase in GC in the DRM in the Gaucher cell model was a secondary accumulation of other lipids, including Cer, DHC, THC, and PG, in which there was a 1.9-, 2.5-, 1.7-, and 2.6-fold increase, respectively. PC, SM, and PI remained relatively unchanged (Fig. 5A). In the soluble domains, there was a 5-fold increase in GC but no secondary increases, with concentrations of Cer, DHC, THC, SM, PC, PG, and PI remaining relatively unchanged (Fig. 5B). Figure 5C shows that along with the increase in GC in the DRM in the Gaucher cell model came a proportional decrease in the other lipids, such that the composition of the DRM changed. GC now replaced PC as the most-abundant lipid in the DRM, comprising 55% of the DRM, with PC, SM, and Cer comprising only 24%, 11%, and 5%, respectively (Fig. 5C). Analysis of the DRM isolated from the lysosomes of the Gaucher cell model showed a lipid composition similar to that of the total cell DRM, and GC, PC, SM, Cer, and PI were

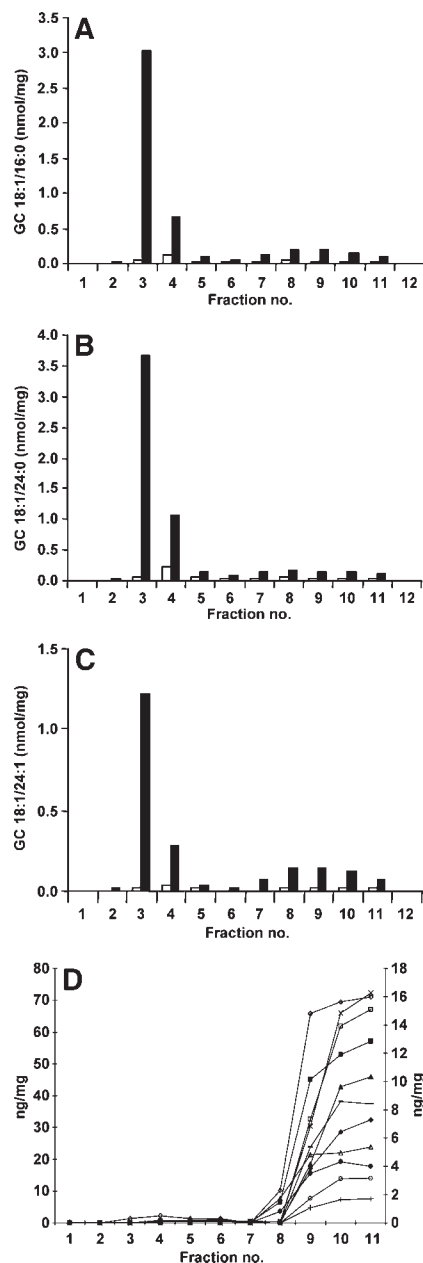


**Fig. 4.** Distribution of GC and lysosomal proteins in the membrane microdomains of the Gaucher disease cell model. The concentration of individual GC species 18:1/16:0 (A), 18:1/24:0 (B), and 18:1/24:1 (C) are shown in membrane microdomains in untreated THP-1 macrophages (open bars) and in the Gaucher cell model (closed bars). Results are expressed in nanomoles of GC per milligram of total protein loaded onto the sucrose gradient prior to fractionation. The distribution of 11 lysosomal proteins was also determined across the membrane microdomain gradient using a multiplex immune quantification assay (D).  $\beta$ -Glucosidase (closed squares), LAMP-1 (open diamonds), saposin C (open triangles),  $\alpha$ -iduronidase (open circles), sulphamidase (closed triangles), iduronate-2-sulphatase (-), acid sphingomyelinase (closed circles),  $\alpha$ -galactosidase (x), arylsulphatase A (open squares), *N*-acetylgalactosamine-4-sulphatase (+), and  $\alpha$ -glucosidase (closed diamonds) all reside in the detergent-soluble fractions. Results are expressed as nanograms of lysosomal protein per milligram of total protein loaded onto the sucrose gradient prior to fractionation.  $\alpha$ -Glucosidase,  $\beta$ -glucosidase, and  $\alpha$ -galactosidase are displayed on the left-hand axis with the remaining proteins on the right-hand axis.

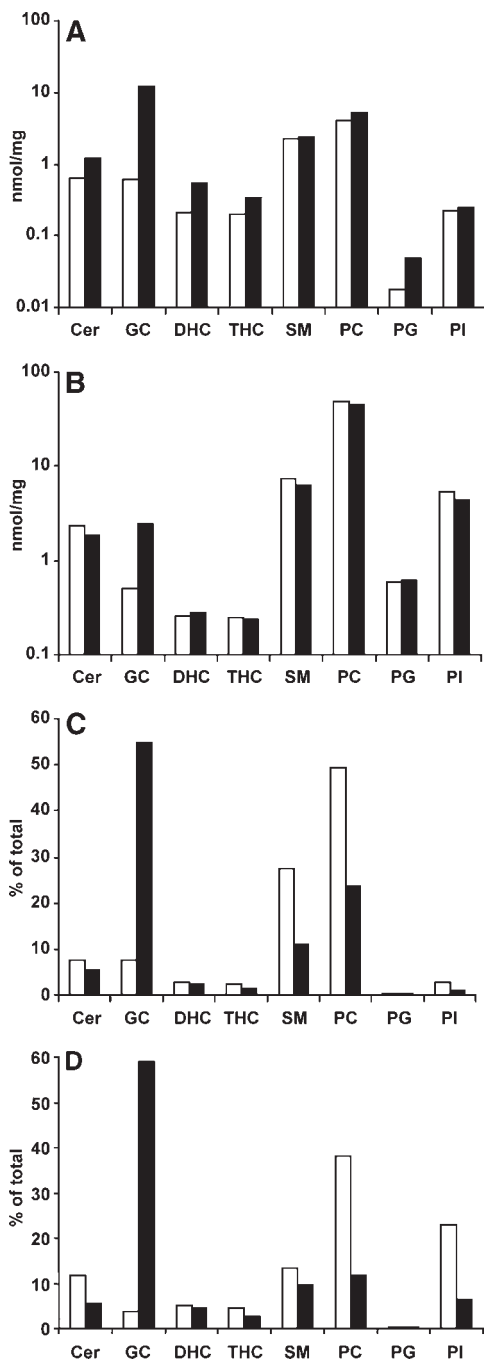


**Fig. 5.** Lipid composition of DRM and soluble membrane domains. The total amount of each lipid present in fractions 3 and 4 (DRM, see Fig. 1) and in fractions 7 to 12 (soluble membrane microdomains) were summed and are shown in A and B, respectively. Results are expressed as nanomoles per milligram of total protein loaded onto the sucrose gradient prior to fractionation. The total amount of each lipid present in the DRM isolated from total cells and the lysosomes after subcellular fractionation were summed, and each lipid type was expressed as a percentage of the total (C, D, respectively). The amount (A, B) and percent (C, D) of Cer, GC, DHC, THC, SM, PC, PG, and PI are shown in untreated THP-1 macrophages (open bars) and the Gaucher cell model (closed bars).

the major lipid species present (59%, 12%, 10%, 6%, and 6%, respectively) (Fig. 5D), although these lipids were considerably reduced in the former.

In the DRM, individual fatty acid species of Cer differed in their distribution. **Figure 6A** shows that in untreated THP-1 macrophages, 14% of Cer 18:1/16:0 was present in the DRM, with another 81% in the soluble membrane domain fractions. The distribution of Cer 18:1/24:0 was different, with 35% in the DRM and 58% in the soluble membrane fractions (Fig. 6B). In the Gaucher cell model, the percentage of Cer 18:1/16:0 and 18:1/24:0 increased in the DRM fractions to 30% and 52%, respectively, with a concomitant decrease in the soluble domains. The Cer 18:1/24:1 had the same distribution as 18:1/16:0 and increased from 16% to 33% in the DRM, and the minor species, 18:1/20:1, 18:1/23:0, and 18:1/23:1, also increased (data not shown). The 18:1/20:0 was present in negligible amounts and remained constant (data not shown).

The PC 32:1, 34:2, 36:2, 36:4, and 38:4 were almost exclusively found in the soluble membrane domains; an example of this is shown in Fig. 6C for PC 34:2. Only 3% of PC 34:2 was present in the DRM, with 96% residing in the soluble domains, and this proportion remained relatively unchanged in the Gaucher cell model. The PC 32:1, 36:2, 36:4, and 38:4 species showed the same distribution as PC 34:2, although 6% of PC 32:1 was present in the DRM (data not shown). However, the distribution of PC 32:0 was different, with 37% present in the DRM and 56% in the soluble domains (Fig. 6D). In the Gaucher cell model, the amount of PC 32:0 increased to 47% in the DRM, with a corresponding decrease to 48% present in the soluble domains. The PC 34:1 species was also present in the DRM, but the majority (92%) was present in the soluble domains (data not shown). In the Gaucher cell model, the amount of PC 34:1 increased to 8% in the DRM, with 90% in the soluble domains. The slight increase in total PC in the DRM in the Gaucher cell model (Fig. 5A) was due to the 1.4-fold increase of PC 32:0 and the 1.2-fold increase of PC 34:1 in the DRM (Fig. 6D and data not shown).

## DISCUSSION

We isolated DRM from THP-1 macrophages based on their insolubility in nonionic detergents (23, 24) as well as their low buoyant density, and identified them using a typical raft marker protein, flotillin 1 (Fig. 1A). Although not all of the proteins in rafts are detergent insoluble, this approach enables an analysis of the lipid composition of the detergent-resistant membrane rafts and the detergent-soluble membrane microdomains in cells. The DRM were shown to be enriched in cholesterol (Fig. 1B), SM, and PC (Fig. 2A). Furthermore, the polyunsaturated species of PC were also present in the soluble domains rather than the DRM (Fig. 3F). Of the sphingolipids, Cer, GC, DHC, and THC associated with the DRM, we observed the characteristic pattern of saturated fatty acid species predominating in the DRM, with the monounsaturated longer chain fatty

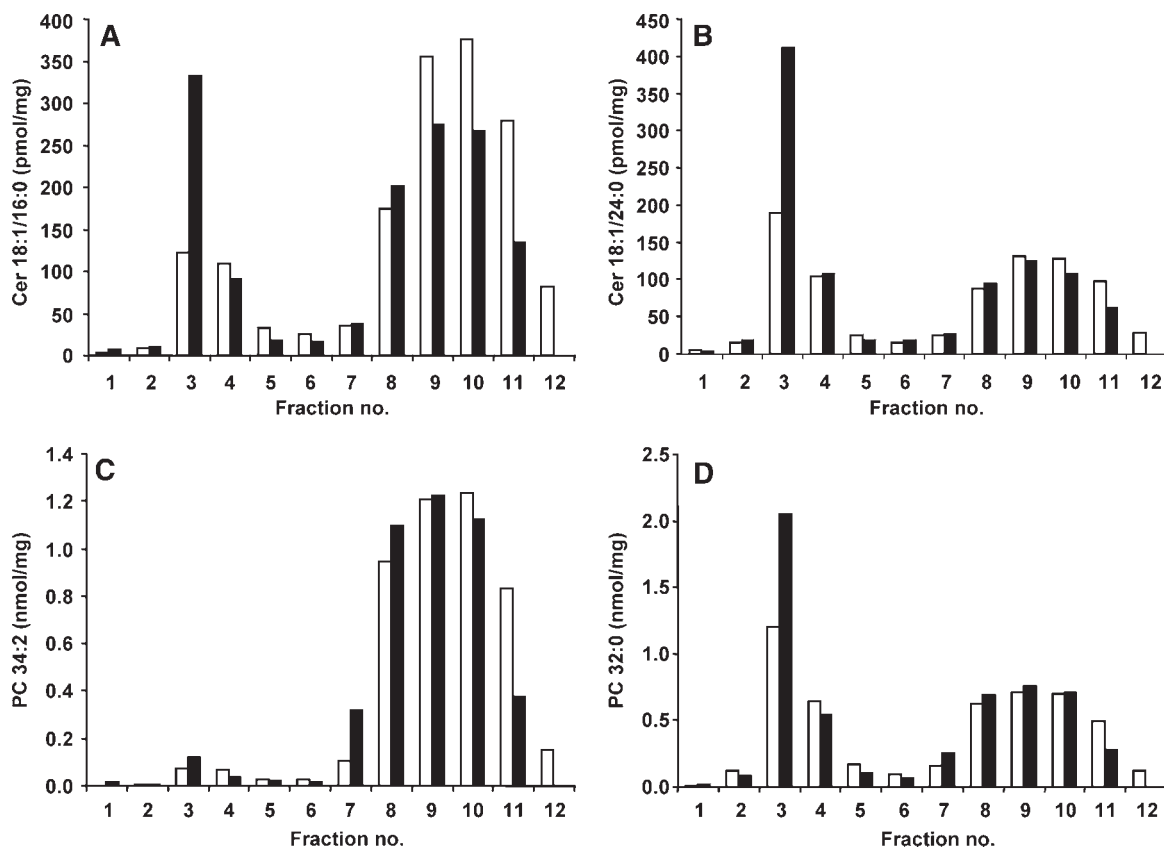


**Fig. 6.** Individual fatty acid species in the membrane microdomains of the Gaucher cell model. Membrane microdomains were isolated from the Gaucher cell model, and individual species of Cer 18:1/16:0 (A) and 18:1/24:0 (B), and PC 34:2 (C) and 32:0 (D) are shown in untreated macrophages (open bars) and in the Gaucher cell model (closed bars). Results are expressed as picomoles or nanomoles of lipid per milligram of total protein loaded onto the sucrose gradient prior to fractionation.

acid derivatives virtually precluded (Fig. 3A–D). This composition of DRM in the THP-1 macrophages is consistent with previous reports of DRM enrichment in saturated sphingolipids and phospholipids (25, 26).

Here, we have shown that the lipid composition of DRM is altered as a direct consequence of the inability of the cell to degrade GC. Previously, we established a macrophage model of Gaucher disease and demonstrated that apart from increased cellular concentrations of GC, Cer, DHC, THC, and PG were also elevated (16). From this study, we demonstrate that this accumulation of GC is primarily in the DRM rather than in the soluble domains, replacing PC as the most abundant lipid in the DRM (Fig. 5C). Consequently, half the proportion of PC and SM and two-thirds the proportion of Cer were present in the DRM (Fig. 5C). The secondary increases in Cer, DHC, THC, and PG were also in the DRM (Fig. 5A), and measuring the individual fatty acid species showed that all species, even those such as Cer 18:1/16:0 (Fig. 6A and data not shown) that were present in low concentrations in the DRM, were elevated. Interestingly, no increase was observed in the relative amounts or the distribution of cholesterol, as well as the concentrations of SM and PC in the DRM of the Gaucher cell model. However, the fully saturated PC 32:0 did increase in the DRM (and to a lesser extent the PC 34:1 species), whereas the other partially


saturated PC species that were virtually excluded from the DRM in the untreated macrophages remained so in the Gaucher cell model (Fig. 6C, D). Thus, there appears to be a general increase of lipids in the DRM in the Gaucher cell model rather than an alteration in the distribution of individual fatty acid species, with no change in the distribution of cholesterol.

It would seem unlikely that the physical properties of the DRM have altered in the Gaucher macrophages, because the exclusion of unsaturated acyl chains would preserve the ordered integrity of the domains (27). This is supported by the finding that the raft domains in the Gaucher macrophages display the same detergent resistance and sucrose buoyancy as ordinary macrophages. Furthermore, although the sphingolipid and phospholipid composition of membrane rafts is altered in the Gaucher cell model, there is no increase in cholesterol. This may be the result of limited external sources of cholesterol in this model system, inasmuch as studies on Gaucher fibroblasts have shown endosomal accumulation of free cholesterol when an exogenous source is available (28). Cholesterol is believed to provide structural support by keeping the membrane rafts together, having a high affinity for sphingolipids rather than the unsaturated phospholipids (6). Therefore, our data would suggest that membrane rafts are not dissociated in Gaucher disease macrophages, but



rather their function is impaired due to alterations in phospholipid and sphingolipid composition.

It is unclear at this stage what effects an altered composition of DRM has on cell function in the Gaucher cell model and how this may lead to disease. What is clear is that lysosomal accumulation of GC does affect other sphingolipids, and a possible hypothesis is one that describes a “jamming of the endosomal system” (12). This hypothesis suggests that GC accumulation in late endosomal membrane rafts causes cholesterol to be “trapped” in these organelles, with the subsequent accumulation of other sphingolipids, ultimately leading to a jam in the membrane raft transport system (12, 29, 30). This trapping of lipids in the late endosome could be caused by the preferential association of sphingolipids with cholesterol, which is a driving force for raft assembly. Raft lipid accumulation is likely to alter the properties of the late endosomal/lysosomal membranes, which will flatten the highly curved internal membranes and interfere with the normal sorting and trafficking abilities of the endosomal system (12). We isolated DRM from lysosomes and showed that their lipid composition was similar to that isolated from total cells in the Gaucher cell model (Fig. 5C, D, respectively); however, the amounts of each of the individual lipid species were much lower in the lysosomal DRM, compared with the total cell DRM, suggesting that although there may be some contamination of the DRM from the lysosomes, it does not account for the entire altered lipid composition. It is noteworthy that none of the lysosomal proteins were found in the DRM, which may suggest that the secondary lipid accumulation is refractory to lysosomal degradation (Fig. 4D). Nonetheless, this finding must be treated with caution; it may be that the lysosomal proteins are neither detergent resistant nor sucrose buoyant and therefore fall to the bottom of the gradient.

It should be noted that we used ESI-MS/MS to quantify individual lipid species, whereas the absolute quantification requires either deuterated internal standards for each lipid species measured or calibration curves for each species to calculate response ratios for the different acyl chain lengths. Because of the current lack of availability of deuterated and single-acyl-chain species for these lipids, this was not possible. We have used one internal standard for each lipid type and therefore cannot rule out experimental error due to differences in responses caused by the different lengths of the carbon chains of the lipid species and the internal standard. Further, for cholesterol determination, we used a cholesteryl ester as the internal standard, and because of the obvious structural differences, we have only reported relative levels. An additional limitation of this study is the use of a cell model generated from a macrophage cell line originating from human leukemia with a Gaucher phenotype induced using a chemical inhibitor (conduritol B epoxide) to inhibit acid  $\beta$ -glucosidase activity within the cell. Although not likely, it cannot be dismissed that the use of a chemical inhibitor may have other unknown actions on the cell and that therefore the changes observed here may not necessarily reflect or exactly mimic the disease state in humans. 

The authors would like to thank Caroline Dean and Debbie Lang for the multiplex immune quantification assays and Peter Sharp for helpful discussions.

## REFERENCES

1. Brown, D., and E. London. 2000. Structure and function of sphingolipid- and cholesterol-rich membrane rafts. *J. Biol. Chem.* **275**: 17221–17224.
2. Pike, L. J. 2006. Rafts defined: a report on the Keystone symposium on lipid rafts and cell function. *J. Lipid Res.* **47**: 1597–1598.
3. London, E. 2002. Insights into lipid raft structure and formation from experiments in model membranes. *Curr. Opin. Struct. Biol.* **12**: 480–486.
4. Pike, L. J. 2003. Lipid rafts: bringing order to chaos. *J. Lipid Res.* **44**: 655–667.
5. Saltiel, A. R., and J. E. Pessin. 2003. Insulin signaling in microdomains of the plasma membrane. *Traffic.* **4**: 711–716.
6. Simons, K., and D. Toomre. 2000. Lipid rafts and signal transduction. *Nat. Rev. Mol. Cell Biol.* **1**: 31–39.
7. Brown, D., and E. London. 1998. Functions of lipid rafts in biological membranes. *Annu. Rev. Cell Dev. Biol.* **14**: 111–136.
8. Kolter, T., and K. Sandhoff. 2006. Sphingolipid metabolism diseases. *Biochim. Biophys. Acta.* **1758**: 2057–2079.
9. Chen, C. S., M. C. Patterson, C. L. Wheatley, J. F. O'Brien, and R. E. Pagano. 1999. Broad screening test for sphingolipid-storage diseases. *Lancet.* **354**: 901–905.
10. Puri, V., R. Watanabe, R. D. Singh, M. Dominguez, J. C. Brown, C. L. Wheatley, D. L. Marks, and R. E. Pagano. 2001. Clathrin-dependent and -independent internalization of plasma membrane sphingolipids initiates two Golgi targeting pathways. *J. Cell Biol.* **154**: 535–547.
11. Puri, V., R. Watanabe, M. Dominguez, X. Sun, C. L. Wheatley, D. L. Marks, and R. E. Pagano. 1999. Cholesterol modulates membrane traffic along the endocytic pathway in sphingolipid-storage diseases. *Nat. Cell Biol.* **1**: 386–388.
12. Simons, K., and J. Gruenberg. 2000. Jamming the endosomal system: lipid rafts and lysosomal storage diseases. *Trends Cell Biol.* **10**: 459–462.
13. Nix, M., and W. Stoffel. 2000. Perturbation of membrane microdomains reduces mitogenic signaling and increases susceptibility to apoptosis after T cell receptor stimulation. *Cell Death Differ.* **7**: 413–424.
14. Beutler, E., and G. A. Grabowski. 2001. Gaucher disease. *In* The Metabolic and Molecular Basis of Inherited Disease. C. R. Scriver, A. C. Beaudet, W. S. Sly, and D. Valle, editors. McGraw-Hill, New York, NY. 3635–3668.
15. Silience, D. J., V. Puri, D. L. Marks, T. D. Butters, R. A. Dwek, R. E. Pagano, and F. M. Platt. 2002. Glucosylceramide modulates membrane traffic along the endocytic pathway. *J. Lipid Res.* **43**: 1837–1845.
16. Hein, L. K., P. J. Meikle, J. J. Hopwood, and M. Fuller. 2007. Secondary sphingolipid accumulation in a macrophage model of Gaucher disease. *Mol. Genet. Metab.* **92**: 336–345.
17. Lisanti, M. P., Z. L. Tang, P. E. Scherer, and M. Sargiacomo. 1995. Caveolae purification and glycosylphosphatidylinositol-linked protein sorting in polarized epithelia. *Methods Enzymol.* **250**: 655–688.
18. Lowry, O. H., N. J. Rosebrough, A. L. Farr, and R. J. Randall. 1951. Protein measurement with Folin phenol reagent. *J. Biol. Chem.* **193**: 265–275.
19. Laemmli, U. K. 1970. Cleavage of structural proteins during the assembly of the head of bacteriophage T4. *Nature.* **227**: 680–685.
20. Bligh, E. G., and W. J. Dyer. 1959. A rapid method of total lipid extraction and purification. *Can. J. Biochem. Physiol.* **37**: 911–917.
21. Liebisch, G., M. Binder, R. Schifferer, T. Langmann, B. Schulz, and G. Schmitz. 2006. High throughput quantification of cholesterol and cholesteryl ester by electrospray ionization tandem mass spectrometry (ESI-MS/MS). *Biochim. Biophys. Acta.* **1761**: 121–128.
22. Meikle, P. J., D. J. Grasby, C. J. Dean, D. L. Lang, M. Bockmann, A. M. Whittle, M. J. Fietz, H. Simonsen, M. Fuller, D. A. Brooks, et al. 2006. Newborn screening for lysosomal storage disorders. *Mol. Genet. Metab.* **88**: 307–314.
23. Brown, D. A., and J. K. Rose. 1992. Sorting of GPI-anchored proteins to glycolipid-enriched membrane subdomains during transport to the apical cell surface. *Cell.* **68**: 533–544.

24. Schuck, S., M. Honsho, K. Ekroos, A. Shevchenko, and K. Simons. 2003. Resistance of cell membranes to different detergents. *Proc. Natl. Acad. Sci. USA*. **100**: 5795–5800.
25. Brown, D., and E. London. 1998. Structure and origin of ordered lipid domains in biological membranes. *J. Membr. Biol.* **264**: 103–114.
26. Pike, L. J., X. Han, K-N. Chung, and R. W. Gross. 2002. Lipid rafts are enriched in arachidonic acid and plasmeneylethanolamine and their composition is independent of caeolvin-1 expression: a quantitative electrospray ionization/mass spectrometric analysis. *Biochemistry*. **41**: 2075–2088.
27. Megha, P. Sawatzki, T. Kolter, R. Bittman, and E. London. 2007. Effect of ceramide *N*-acyl chain and polar headgroup structure on the properties of ordered lipid domains (lipid rafts). *Biochim. Biophys. Acta*. **1768**: 2205–2212.
28. Salvioli, R., M. Tatti, S. Scarpa, S. M. Moavero, F. Ciaffoni, F. Felicetti, C. R. Kaneski, R. O. Brady, and A. M. Vaccaro. 2005. The N370S (Asn<sup>370</sup>→Ser) mutation affects the capacity of glucosylceramidase to interact with anionic phospholipid-containing membranes and saposin C. *Biochem. J.* **390**: 95–103.
29. van Meer, G., and Q. Lisman. 2002. Sphingolipid transport: rafts and translocators. *J. Biol. Chem.* **277**: 25855–25858.
30. Pagano, R. E. 2003. Endocytic trafficking of glycosphingolipids in sphingolipid storage diseases. *Philos. Trans. R. Soc. Lond. B Biol. Sci.* **358**: 885–891.